frontiers | Frontiers in Marine Science

ORIGINAL RESEARCH
published: 09 June 2022
doi: 10.3389/fmars.2022.910125

Holocene Environmental Evolution Response to the Human Activities and East Asian Summer Monsoon Variation in the Liangzhu Ancient City Complex, Eastern China

Chunhui Zou[1], *Longjiang Mao*[1,2*], *Siwei Shan*[3*], *Shuangping Zhaocheng*[4] *and Duowen Mo*[4]

[1] Institute of Scientific and Technical History, Nanjing University of Information Science and Technology, Nanjing, China, [2] School of Marine Science, Nanjing University of Information Science and Technology, Nanjing, China, [3] Department of Archaeology, School of History, Wuhan University, Wuhan, China, [4] College of Urban and Environmental Sciences, Peking University, Peking, China

OPEN ACCESS

Edited by:
Joseph Carlin,
California State University, Fullerton, United States

Reviewed by:
Xinxin Zuo,
Fujian Normal University, China
Li Wu,
Anhui Normal University, China

***Correspondence:**
Longjiang Mao
mlj1214@nuist.edu.cn
Siwei Shan
swshan@whu.edu.cn

Specialty section:
This article was submitted to Coastal Ocean Processes, a section of the journal Frontiers in Marine Science

Received: 31 March 2022
Accepted: 09 May 2022
Published: 09 June 2022

Citation:
Zou C, Mao L, Shan S, Zhaocheng S and Mo D (2022) Holocene Environmental Evolution Response to the Human Activities and East Asian Summer Monsoon Variation in the Liangzhu Ancient City Complex, Eastern China. Front. Mar. Sci. 9:910125. doi: 10.3389/fmars.2022.910125

The Liangzhu Ancient City Complex is located in a low-lying coastal delta area, and its environmental evolution would have had a significant impact on the human-environment interactions. In this study, element geochemistry and grain size of the sediment sequence from a dam section in Ganggongling (GGL) reveal crucial aspects of sedimentary dynamics, environmental evolution, human activities, and East Asian Summer Monsoon (EASM) variation in the Liangzhu area since 5500 a. Starting from the middle-to-late Holocene, the GGL section shows an overall transition from warm humidity to cold-dry, which is consistent with the climate record dimension in southern China. Through comprehensive analysis of the sedimentary environment before and after the dam's completion, it can be found that the Ganggongling dam has played a positive role in regulating mountain torrents and met the needs of production and domestic water, such as rice planting through water storage. Further applications on the multi-decadal to centennial time scale demonstrate that variations in solar activity may control the EASM intensity mainly in southern China, which is subject to ENSO intensity changes.

Keywords: environmental evolution, human activities, East Asian summer monsoon, Liangzhu Ancient City Complex, dam section

INTRODUCTION

The river basins and their deltas are areas that are very sensitive to global and regional climate and environmental changes, and their environmental changes have largely influenced and constrained the rise and fall of civilizations in these areas during historical periods (Zong et al., 2007; Rolett et al., 2011; Timmermann and Friedrich, 2016; Dong et al., 2019). Studying environmental changes in estuaries and deltas and the corresponding adaptation and response to human activities has become a central issue of widespread scholarly interest in the past decades. Previous studies have primarily

focused on the relationship between climate and vegetation and human activities in environmental elements, as well as sudden disaster events that have a direct impact on human activities, such as earthquakes and floods (Cullen et al., 2000; Yi et al., 2003; González-Sampériz et al., 2008; Kennett et al., 2012; Amorosi et al., 2013; Dixit et al., 2014; Sun et al., 2019). In addition, the hydrogeomorphic environment, such as sea-level change and river and lake evolution, are closely related to human activities, and their evolutionary processes significantly affect the activities of ancient humans, which also become a current research hotspot (Turney and Brown, 2007; Chen et al., 2008; Innes et al., 2014; Nienhuis et al., 2020). For example, in the Atacama desert region of northern Chile, the Mississippi River basin, and the Nile River basin, cultural decline at certain times has been attributed to several events of the river, lake, and floodplain shrinkage and reduced river flows (Núñez et al., 2002; Kidder et al., 2008; Macklin et al., 2015; Munoz et al., 2015). Thus, understanding past human-nature interactions is essential for exploring long-term human culture and agriculture and provides important information for human adaptation to future climate change.

As an important component of the global climate system, the East Asian monsoon affects nearly 60% of the world's inhabitants (Yao et al., 2015). Only by studying the response of the East Asian monsoon to the overall behavior of the global climate system in the framework of global change can we fully understand the patterns and mechanisms of the East Asian monsoon climate change. In recent years, scholars have reconstructed the Holocene monsoon climate and environmental characteristics of different regions, divided them into stages and analyzed the relationship between the environment and monsoon evolution (Kutzbach, 1981). In addition, the historical evolution of the East Asian Summer Monsoon (EASM) has been extensively studied using a variety of geological archives, including loess-paleosol sequences, marine and lake sediments, peat sediments, and stalagmites, revealing the cycle of changes in the East Asian Monsoon and its driving mechanisms (Huang et al., 2018; Liu et al., 2013; Mu et al., 2016; Goldsmith et al., 2017; Gai et al., 2020; Li et al., 2022). Geochemical elements in lacustrine sediments can provide a continuous, high-resolution record of changes in terrestrial and aquatic ecosystems (Colman et al., 2007; Fu et al., 2013). Geochemical elements also provide key information on environmental changes in lakes, such as erosion history and soil and slope cover formation processes, as well as the climate history of continental areas and regional responses to large-scale climate change, which can then be used to infer climate conditions (Oldfield et al., 1979; Rosenbaum and Reynolds, 2004). However, the reconstruction of the East Asian Summer Monsoon in eastern China relies heavily on high-resolution oxygen isotope records preserved in cave stalagmites. This is because stalagmites grow in closed and stable cave systems, and the environmental information obtained is fidelity-rich and sensitive to environmental changes. Therefore, we urgently need other higher resolution proxies (e.g., geochemical elements, etc.) to enhance the understanding of the East Asian summer monsoon in eastern China.

The Neolithic culture of the lower Yangtze River region, one of the birthplaces of Chinese culture, has undergone a long and complex development process in the Holocene (Stanley and Chen, 1996). As the last stage of the prehistoric culture in the region, Liangzhu culture is famous for its rice cultivation and large water engineering constructions, representing the pinnacle of the Neolithic culture in the lower Yangtze River region (Liu B et al., 2017a). The Liangzhu site was also inscribed on the UNESCO World Heritage List in 2019. Geographically, the Liangzhu area is located in a low-lying coastal area on the north coast of Hangzhou Bay, which is significantly affected by the East Asian monsoon and is also highly susceptible to extreme climatic and environmental events such as typhoons, storms, floods, and seawater intrusion, and scholars consider this as a possible reason for the interrupted disappearance of Liangzhu culture (Nicholls and Cazenave, 2010; Kirwan and Megonigal, 2013; Fan et al., 2017). During the Liangzhu culture, more evergreen, moisture-loving genera, such as *Cyclobalanopsis Oerst* and *Castanopsis armata*, were found in the sporulation record, reflecting a climate that remained warm and humid in general (Wang and Zhang, 1981; Shi, 2011). However, systematic studies on the Holocene environmental evolution and monsoonal changes in the Liangzhu area are lacking. In recent years, archaeological work has revealed the existence of a large and complex hydraulic system at the periphery of the ancient city of Liangzhu, consisting of a group of nearly ten dams of different sizes stacked in the ravine between the mountains, which range in age from the early to the middle of the Liangzhu culture (Wang and Liu, 2015; Huan et al., 2022). However, little research has been conducted on the Holocene environmental evolution process within the dam system and the environmental significance of prehistoric dams. For this purpose, we selected Ganggongling Dam, one of the closest dams in the high dam system to the Hangjiahu Plain, and analyzed the sediment sequence by stratigraphy, sedimentology, chronology, and geoarchaeology of the sediments sampled from the reservoir area within the dam. The resulting lithology, geochemical element abundance, and grain size distribution were obtained and compared with other regional proxies. The objectives are 1) to recover the Holocene environmental evolution of the reservoir area, 2) to discuss the environmental significance of prehistoric dams and their relationship with human activities, and 3) to reconstruct the regional precipitation processes and to explore their relationship with changes in EASM intensity.

REGIONAL SETTING

The Hangzhou-Jiaxing-Huzhou Plain (Hangjiahu Plain) is part of the southern Yangtze River Delta, bordered by Taihu Lake in the north, the hilly areas of western Zhejiang in the west, Qiantang River and Hangzhou Bay in the south, and Wujiang to Jinshan in the east, and is an alluvial plain of rivers and lakes with low topography and a dense network of waterways (**Figure 1B**). The overall topography of the region is not very undulating, with elevations generally ranging from 2 to 4 m. The

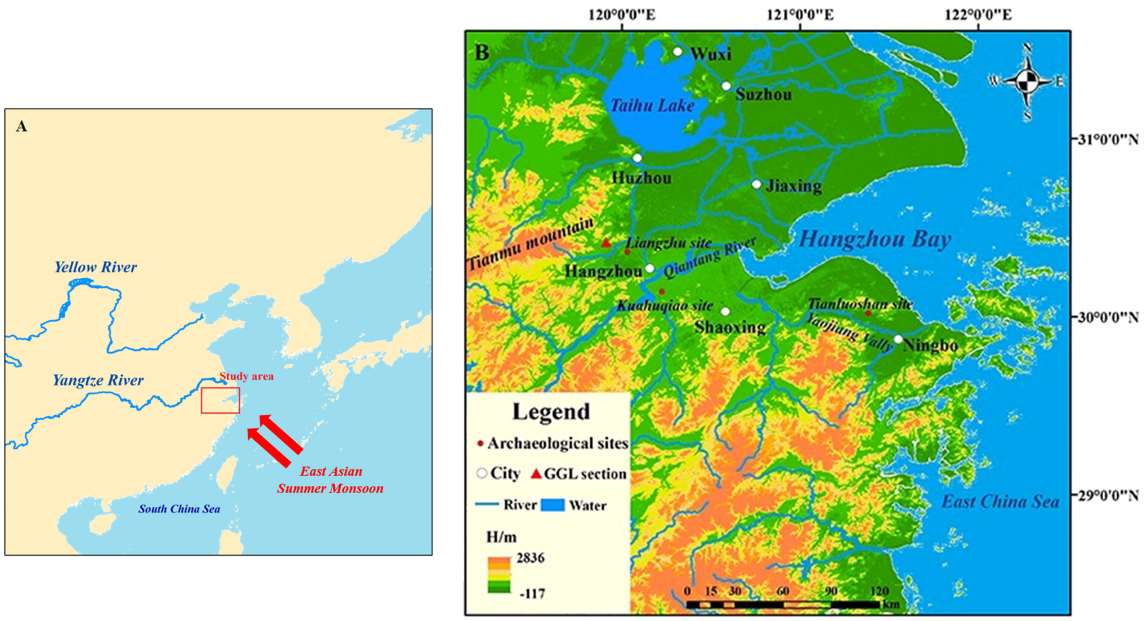

FIGURE 1 | **(A)** Location of the study area in the lower reaches of Yangtze River; **(B)** Specific location of the GGL profile and its surrounding hydrogeomorphology.

elevation is lower in the northeast in the area in front of Tianmu Mountain and slightly higher in the southwest along the Qiantang River and Hangzhou Bay, with a general pattern of high in the southwest and low in the northeast (Yang et al., 2002). The surface sediments of the region are dominated by river-lake phase sediments composed of fine-grained clay and silt from the Yangtze River, Qiantang River, and numerous lakes, and the tidal flats phase sediments with coarser grains and loose soils on the southern edge (Lu, 2008). The study area of Liangzhu City is located between Dazhe Mountain and Daguan Mountain south of the Tiaoxi River, bordering some low mountains on the western and southwestern edges of the Hangjiahu Plain.

The Hangjiahu Plain has a well-developed water system, and most of the rivers have a small watershed area, short headwaters, and fast flow rates. Most of the water systems originate from Tianmu Mountain and Mogan Mountain, among which the Tiaoxi River belongs as one of the eight major water systems in Zhejiang Province (Yan et al., 1959; Xu, 2012). The climate of the Hangjiahu Plain is an East Asian monsoon climate with an uneven seasonal distribution of precipitation, with low rainfall in spring and winter and high precipitation in summer and autumn (**Figure 1A**). The average annual temperature in the region is 15~16°C, and the average yearly precipitation is 1000~1400mm.

MATERIALS AND METHODS

Section Recovery and Dating

Ganggongling Dam is at the easternmost end of the high dam system at the periphery of the ancient city of Liangzhu, located in Banyao Town, Hangzhou, Zhejiang Province. The exploratory pit shows a uniform dam body with artificial accumulation, which shows that the northern slope of the dam body slopes to the north. We took a natural sediment profile inside the dam on the north side of the dam accumulation, and the depth of the profile exceeded 227 cm without bottoming out, which is called the Ganggongling section (30°25′11″N,119°54′39″E; elevation:10m). Samples spaced 2-5 cm apart were selected for further laboratory analysis, yielding a total of 63 samples.

Photos of the GGL profile are shown in **Figure 2A**. According to the detailed lithological description, grain size distribution, and sediment structure, the GGL section can be divided into eight layers from top to bottom. The detailed description is as follows:

Zone 1 (0~22cm) is the surface paddy soil, mainly composed of gray clayey silt with some rusty brown root-whisker-like rust spots. Zone 2 (22~42cm) is the bottom of paddy soil in the upper part, which is gray clayey silt; the lower part is brownish yellowish, grayish-brown clayey silt, with undulating upper and lower interfaces. Zone 3 (42~93 cm) is brownish-gray clayey silt with rusty brown root-whisker-like rusty spots. Zone 4 (94~122 cm) and zone 5 (122~150 cm) are dark gray to grayish-brown mottled clayey silt and dark gray clayey silt, respectively. Zone 6 (122-150 cm) comprises grayish-green clayey silt and rusty yellow clayey silt. Zone 7 (203-227 cm) and Zone 8 (227 cm~) are gray clayey silt sand with brownish-yellow clayey sand and gray clayey sand with brown spots.

The photoluminescence dating was done by the Laboratory of Environmental Archaeological Photoluminescence, Institute of Geography, Henan Provincial Academy of Sciences. 4-11um quartz particles were obtained by the conventional pretreatment method for all samples, and quartz equivalent

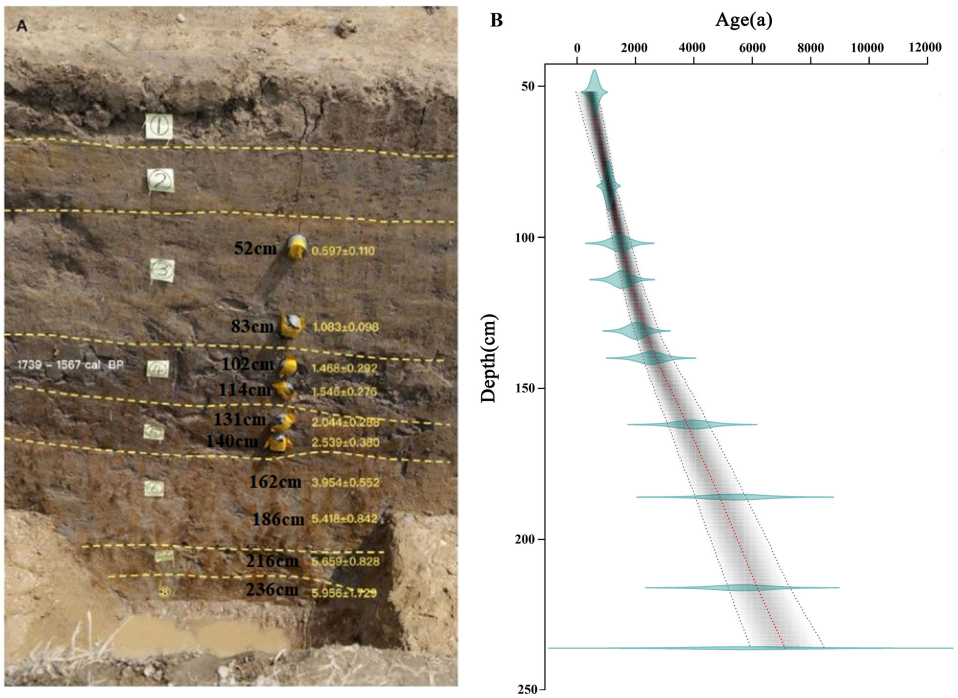

FIGURE 2 | Stratigraphy **(A)** and age-depth model **(B)** of the GGL section.

dose (De) was tested by the single piece regenerative dose method (SAR). U, Th, and K contents were tested by neutron activation method (NAA) in the Analysis and Testing Research Center of Beijing Institute of Nuclear Industry and Geology. Water content was measured by actual water content, the absolute error of 5% was given, and dose recovery experiments at different temperatures were conducted for all samples (Lai and Brückner, 2008). A 7.5 mm thick Hoya U-340 filter was placed between the photomultiplier tube (PMT) and the sample at the top of the photoluminescence system to remove the irradiated light. De measurements were performed by the single slice regenerative dose (SAR) method (Banerjee et al., 2001). Based on the improved experimental procedure of Murray et al., the "cutheat preheat" was changed to "110°C thermoluminescence (TL) measurement". The purpose of the improvement is twofold: one is to release the thermal instability signal, and the other is to use the information of the quartz 110°C TL signal peak to examine the sensitivity change during the experiment.

Abundance of Elements

The samples were tested for macronutrients and trace geochemical elements by the Key Laboratory of the Ministry of Education for Orogeny and Crustal Evolution, Peking University. The test element is divided into constant elements (e.g., SiO_2, Al_2O_3, Fe_2O_3, TiO_2, etc.) and trace elements (Rb, Sr, Zr, V, etc.). The naturally dried samples were sieved through a 20 mesh sieve, mixed thoroughly, and ground to less than 200 mesh using a ball mill. We took 10~20 g of the mixed sample and sealed it in a sealed bag and send it to the laboratory for testing. FeO was determined by titrimetric method, and other macronutrients and some trace elements were tested by Axios wavelength dispersive X-ray fluorescence spectrometer according to GB/T14506.28-2010 standard. The remaining trace elements were determined using an iCAPRQ inductively coupled plasma mass spectrometer. Concrete steps are as follows: (1) 0.25g sediment sample was weighed and introduced into a Teflon tank matched with the microwave digestion instrument, and heated at 85°C for 20 minutes for pre-digestion; (2) 13 ml of HNO3 and 5 ml of HF were added to the digestion tank, which was ensured to be completely sealed and placed in the microwave digester; (3) After the microwave digestion was carried out and the sample was brought to room temperature, the lid and the inner wall of the digestion tank were rinsed with ultrapure water, 5 mL of $HClO_4$ was added and then heated at 190°C on a special heating plate to remove the acid. (4) When the digestion solution was gradually evaporated to the size of soybean and no white smoke came out, the digestion tank was repeatedly rinsed with 5‰ HNO3 solution and finally diluted to 50mL for testing on the machine.

Grain Size Analysis

The grain size data of the sediment samples were measured and analyzed at the Key Laboratory of the Ministry of Education for Surface Process Analysis and Simulation, School of Urban and Environmental Studies, Peking University, with a laser grain size

analyzer, Mastersize 2000, Malvern, UK, with a resolution of 0.15φ and a measurement range of 0.02~2000 μm with a relative error <3%. Pre-processing work is as the following: (1) in order to remove gravel, plant roots and other biological residues from the samples, naturally air-dried samples were passed through a 20-mesh sieve and 0.3-0.5 g of the sample was placed into a washed and dried 50 ml beaker after all samples were well mixed; (2) 20 ml of 10% H_2O_2 was added to a beaker and heated to 200° C on a hot plate until there was little H_2O_2 left; (3) 10 ml of 10% HCl was added to a heated beaker, the beaker was filled with pure water to room temperature, and the supernatant was removed after standing for 12 hours; (4) 10 ml of 0.05 mol/L (NaPO3)6 was added to the sample, placed in the ultrasonic shaker for 10 minutes and then put into the machine for testing.

RESULTS

OSL Dating Results

The ten OSL dates from the GGL section are provided in **Table 1**. The calculated ages of the GGL profiles range from 6000 to 400a BP (**Figure 2B**). GGL-OSL-07 and GGL-OSL-08 differ in depth by only 24 cm but span in age from 3954 ± 552 a to 5418 ± 842 a, with depositional interruptions that may be due to erosion or artificial dredging.

Abundance of Elements

As shown in **Figure 3**, the relative contents of major elements are represented by the counterparts of their oxides. Al_2O_3, Fe_2O_3, and SiO_2 dominate the sediments in the depositional sequence of

TABLE 1 | OSL dating results for samples in the CY section.

Lab.N	Sample N.	Depth(cm)	Rb /ppm	U /ppm	Th /ppm	K /%	Q-De(Gy)	w.c(%)	Q-Dose rate(mGy/a)	Q-Age(ka)
L536	GGL-01	52	132±3.4	3.81±3.6	14.5±2.1	1.97±0.55	2.47±0.02	19.93	4.139±0.761	0.597±0.110
L537	GGL-02	83	131±0.7	3.86±1.2	15.1±1.7	2.10±0.35	4.54±0.03	20.81	4.193±0.379	1.083±0.098
L538	GGL-03	102	137±1.3	4.02±3.3	15.8±2.6	1.82±0.79	5.76±0.03	24.18	3.925±0.780	1.468±0.292
L539	GGL-04	114	143±2.6	4.17±4.2	16.6±3.4	2.03±0.26	6.58±0.03	22.69	4.256±0.760	1.546±0.276
L540	GGL-05	131	139±2.1	4.07±2.9	16±1.3	1.98±0.39	8.52±0.02	21.91	4.167±0.587	2.044±0.288
L541	GGL-06	140	142±2.3	4.41±3.2	16.5±2.5	1.82±0.32	10.33±0.04	24.38	4.068±0.608	2.539±0.380
L542	GGL-07	162	152±2.1	4.2±2.6	17.3±2.7	1.93±0.48	16.95±0.08	21.28	4.286±0.598	3.954±0.552
L543	GGL-08	186	155±3.0	4.08±1.6	16.6±3.1	2.12±0.84	23.35±0.09	22.30	4.310±0.670	5.418±0.842
L544	GGL-09	216	146±2.9	3.63±2.9	15.2±2.9	2.03±0.36	23.01±0.13	20.51	4.066±0.594	5.659±0.828
L545	GGL-10	236	138±3.6	3.26±5.4	14.1±2.4	1.94±0.88	22.48±0.12	21.07	3.774±1.096	5.956±1.729

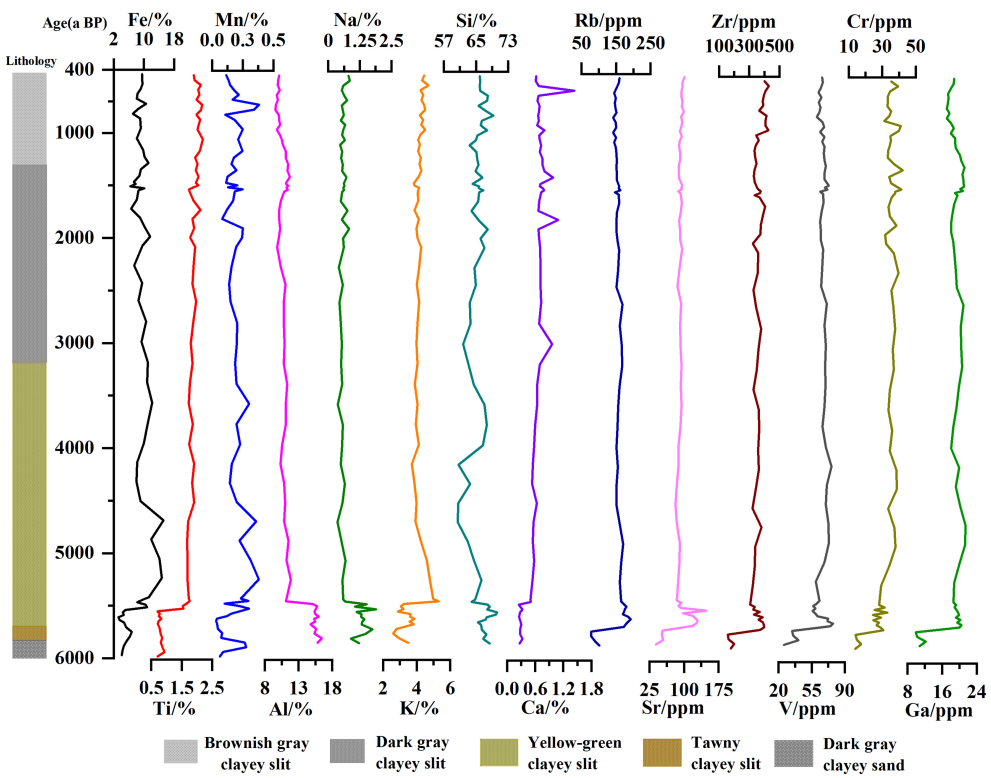

FIGURE 3 | Stratigraphic sequence and major element concentrations of sediments in the GGL profile.

the GGL profile. The concentration of Al_2O_3 varies between 9.6 and 16.4% (average=11.7%), with maximum values during 219~228cm. Conversely, Fe_2O_3 shows a continuous reduction at the bottom of the section (average=8.54%). Similar to the trend of Al_2O_3, the SiO_2 concentration ranges between 58.6 and 70.3%, with a maximum contribution of 201cm. In terms of the trace elements, Zr, Ti, V, Sr, Cr, and Ga have relatively high average contents. V (77.9 ppm) has the highest average range among the heavy metals, followed by Cr (42.34 ppm). Moreover, the concentration of heavy metals dramatically vary in the top and lower parts of the section, while it is relatively stable in the middle part of the section.

Grain Size Distribution Characteristics

Grain size frequency curves showing multi-peak distribution (**Figure 4A**). The grain size versus standard deviation plot shows that four sensitive grain size components can be identified based on the three standard deviation peaks at 17.4 μm, 79.4μm, and 416.9 μm in the curve (Boulay et al., 2007). Their corresponding size ranges are <45.7μm, 45.7–158.5μm, and >158.5μm, respectively (**Figure 4B**). The grain size analysis results show that the entire section is dominated by silty sand, followed by clay and sand, and the sand content fluctuates significantly from 200 cm onwards (**Figure 4C**). Therefore, we designated three different grain size groups from fine to coarse sensitive fractions 1 (SC1) to 3 (SC3), thus representing three different sensitive grain size fractions. In terms of percentage content, the content of SC1 is dominant, followed by SC2 and SC3. The trend of the median grain size is more similar to SC2 and SC3, while it is negatively correlated with SC1(**Figure 4C**).

DISCUSSION

Climate Interpretation From the Multiproxy Approach

Chemical weathering can alter the mineral composition of the land surface, and the resulting debris constitutes the majority of the clastic fraction in the sediment. Therefore, integrated geochemical element parameters can overcome the uncertainty of a single element's response to the environment and better reflect the degree of chemical weathering of sediments. (Kronberg et al., 1986; Fu et al., 2018; Stankevica et al., 2020). In this paper, the following chemical weathering and precipitation proxies were selected to infer the climate change in the study area since the Holocene.

In lacustrine sediments, the precipitation intensity can be inferred from Fe/Mn. The anaerobic environment created by the water-sediment interface in deep lakes favors the dissolution of iron and manganese (Davison, 1993), while manganese is more likely to precipitate in an oxidizing environment (Boyle, 2002). The relative precipitation can be inferred from lake-level proxies such as Fe/Mn. Therefore, the higher Fe/Mn ratio reflects a decrease in the oxygen content of the water body, indicating a further increase in the degree of anaerobicity of the lake water and a rise in the lake water level. Recent work has also confirmed

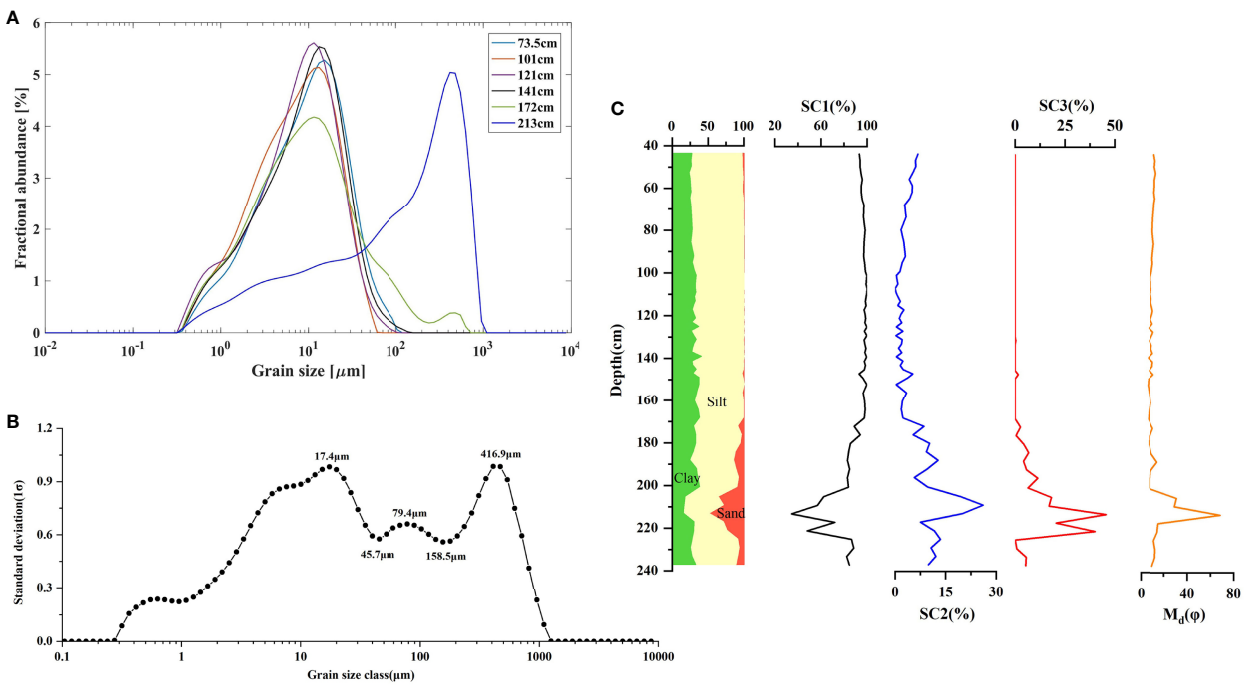

FIGURE 4 | Grain size analysis results in the GGL section. **(A)** Grain size frequency curves at different depths; **(B)** Grain size classification with standard deviation diagram; **(C)** Depth variation of the three grain size sensitive components expressed as relative content.

that lower Fe/Ti and Mn/Ti generally occur in reducing environments because Ti is more stable in depositional environments (Boës et al., 2012), and the reduction of Fe, Mn in reducing environments Sedimentation would decrease further (Moreno et al., 2007; Kylander et al., 2011), which would also represent an increase in precipitation. In the GGL profile, the ratios of Fe/Ti and Mn/Ti show a good correlation, which in turn are negatively correlated with Fe/Mn (**Figures 5A–C**), which may provide insight into the precipitation variation in the dam supporting evidence.

In general, certain major and trace elements (e.g., K, Na, Ca, Al) behave differently during chemical weathering and can therefore be used to trace the intensity of chemical weathering. The chemical weathering index [CIA = $Al_2O_3/(Al_2O_3 + CaO + Na_2O + K_2O)$] is mainly used to reflect the degree of alteration of minerals during the weathering of sediments, and the increase of its value indicates the growth of chemical weathering of minerals (Chen et al., 2020; Perri, 2020; Wang et al.,2020). In addition, Rb, Sr, and Zr are also commonly used in the study of lacustrine sediments. Rb is easily enriched *in situ* by adsorption of clay minerals during chemical weathering or rainfall percolation, while Sr is easily left *in situ* in a free state with surface or groundwater (Jeong et al., 2006; Du et al., 2011; Chang et al., 2013). Zr is mainly found in heavy minerals such as zircon rocks, which are very stable during weathering. Existing studies have shown that with the intensification of chemical weathering, the Rb/Sr value of the *in-situ* residual sediments will gradually increase, while the Zr/Rb value will gradually decrease (Kalinin et al., 2018). Therefore, an enormous Rb/Sr value and a smaller Zr/Rb value can represent a humid environment with high rainfall and intense chemical weathering, and vice versa, a dry environment with weak chemical weathering and low rainfall. The sum of Ti+V+Cr+Zr+Ga elemental hydrolyzates marks the distribution of the landing source material and migrates into the water as part of the coarse suspension, which is positively correlated with the weathering intensity (Ryabogina et al., 2019). The Rb/Sr values in the GGL profiles showed a similar trend to the sum of CIA and Ti+V+Cr+Zr+Ga (r = 0.93, 0.98), which can well reflect the change of weathering intensity (**Figures 5D–G**).

Holocene Paleoenvironmental Evolution of the Liangzhu Area

The Ganggongling Dam is an artificial paleodam-like relic, and the available ^{14}C dating results indicate that it was built around 5000 cal a BP (Wang and Liu, 2015). Before the dam was built (6000~5500aBP), the median grain size curve fluctuated violently, and the grain size was at the coarsest and best-sorted stage in the entire section. This reflects the solid hydrodynamic conditions and frequent river swings at this time, which may have accumulated some flash flood alluvium (**Figure 4C**). After the dam was built (after 5500a BP), the sedimentary environment in the dam was dominated by lacustrine facies, which well recorded the precipitation changes in this area. In this paper,

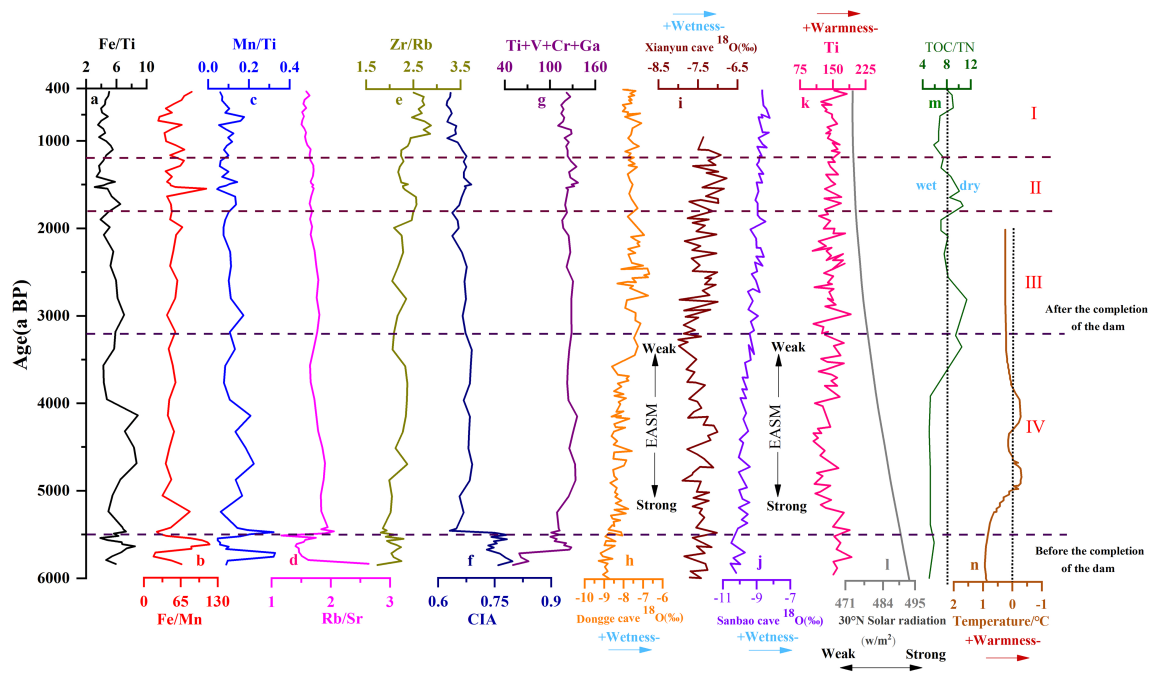

FIGURE 5 | Comparison of EASM records from GGL section **(A–G)** and other monsoon regions records. **(H)** Stalagmite ^{18}O record from the Dongge Cave in China (Dykoski et al., 2005); **(I)** Stalagmite ^{18}O record from the Xianyun Cave in China (Che et al., 2018); **(J)** Stalagmite ^{18}O record from the Sanbao Cave in China (Dong et al., 2013); **(K)** Elemental intensity of Ti in Huguangyan Maar Lake (Wu et al., 2011); **(L)** 30°N June Insolation (Berger and Loutre, 1991); **(M)** Ratio of total organic carbon to total nitrogen (TOC/TN) (Yang et al., 2011); **(N)** Pollen records of Core CM97 (Yi et al., 2003).

lithologic and multi-proxy data from the GGL section is correlated with previously published literature from the study area to reveal detailed paleoenvironmental evolution and monsoonal changes in the Liangzhu region since about 5500a BP. Specifically, the mid-late Holocene paleoenvironmental evolution is grouped into Stage IV ~ Stage I.

Stage IV: From 5500 to 3200 a BP, relatively higher values for the Rb/Sr and Ti+V+Cr+Zr+Ga, with correspondingly high CIA values, indicate more variability in the intensity of chemical weathering, reflecting a humid period (**Figures 5D, F, G**). Similarly, Fe/Mn ratio from GGL sediments is more positive at this stage, possibly reflecting an intensified humidity (**Figure 5B**). During the same interval, the ^{18}O values at the lower levels of Dongge Cave, Xianyun Cave, and Sanbao Cave indicate an increase in precipitation, that is, an enhancement of EASM (**Figures 5H–J**; Dykoski et al., 2005; Dong et al., 2010; Cui et al., 2017). In addition, the lower Ti content in the sediments of Huguangyan Maar Lake also reveals the warm and humid climate conditions (**Figure 5K**; Wu et al., 2011). The TOC/TN values of core CM97 from the Changjiang Estuary, located in the East Asian monsoon region, also recorded an increase in precipitation during the contemporaneous period, likeness to the GGL profile (**Figure 5M**, Yang et al., 2011).

Stage III: Between 3200 and 1800 a BP, the chemical weathering intensity gradually weakened, as indicated by elemental indicators in the GGL section, and an arid climate probably caused this. The CIA values are relatively low, with comparatively small fluctuations (**Figure 5D**). Fe/Mn, Rb/Sr ratios, and Ti+V+Cr+Zr+Ga remained stable and lower, while Zr/Rb, Fe/Ti, and Mn/Ti increased significantly (**Figures 5A–C, E–G**). These data all indicate a considerably dry phase. Grain size evidence suggests that the profile shifts to a less hydrodynamic lacustrine environment (**Figure 4C**). Within this time interval, the increasing rate of the stalagmite $\delta^{18}O$ record from Dongge cave, Xianyun cave, and Sanbao cave provide additional evidence for this dry interval (**Figures 5H–J**; Dykoski et al., 2005; Dong et al., 2010; Cui et al., 2017). Furthermore, a dry period from 3000 to 2000 cal yr BP was also detected in Ti and TOC/TN record from the Huguangyan Maar Lake and core CM97 (**Figure 5K, M**, Wu et al., 2011; Yang et al., 2011). Combined with the weakening of solar radiation, the intensity of EASM in this stage remarkably decreased (Berger and Loutre, 1991).

Stage II: From 1800 to1200a BP, the intensity of chemical weathering is slightly higher than in stage III, but the overall fluctuation is not significant. As indicated by elemental ratios and CIA values in the GGL section, this could be caused by a slightly enhanced warm and humid climate. Similarly, $\delta^{18}O$ values from Dongge cave and Sanbao cave showed a slight decrease in magnitude for this time interval, possibly reflecting the increased wetness (Dykoski et al., 2005; Dong et al., 2010). Previous studies from Yangtze River estuary sediments also confirm that warm and humid climatic conditions occurred around 1500 a BP (Yao et al., 2015; Li et al., 2016). The humid-loving pollen records from the Dianshan Lake and Yangtze River Delta provide further evidence of a warm-humid period since 1800 aBP (Yi et al., 2003; Zhang, 2005; Yi et al., 2006). The intensity of EASM increased slightly in this phase.

Stage I: Between 1200 and 400 a BP, Rb/Sr, Fe/Mn, CIA, and Ti+V+Cr+Zr+Ga were further reduced. Meanwhile, the Fe/Ti, Mn/Ti, and Zr/Rb ratios notably increased. As recorded in these element ratios in GGL sediments, relatively weak chemical weathering is closely related to cold and dry climatic conditions. Similarly, in the Dongge cave and Sanbao cave, a dry climate phase was inferred from the $\delta^{18}O$ record (**Figures 5H–J**; Dykoski et al., 2005; Dong et al., 2010; Cui et al., 2017). The Ti records from Huguangyan Maar Lake also confirm that it was characterized by cold and dry climatic conditions (**Figure 5K**; Wu et al., 2011). The above evidence shows a further weakening of EASM intensity.

Environmental Significance of Dams and the Response of Human Activities

The Liangzhu area is highly influenced by the East Asian summer winds and is also vulnerable to extreme climatic and environmental events, such as typhoons, storms, floods, and seawater intrusion (Fan et al., 2017). From the topographic location, there are several rivers in the northern mountains of the ancient city of Liangzhu. It is not difficult to speculate that when typhoons and storm events occur, flash floods or mudslides are likely to form around the area, which seriously threatens the safety of the ancient city and the ancestors living in Liangzhu (Zong et al., 2012; Long et al., 2014; Wang et al., 2018; Ling et al., 2021). The Gangongling dam in this paper was built in the late Liangzhu culture around 5000 years ago and was abandoned after the Liangzhu culture. Therefore, the environmental significance of the dam can be understood by comparing the changes in the depositional environment of the dam before and after its construction. Before the dam was built (6000-5000a BP), it was a river environment with an unstable depositional environment and a frequently oscillating river channel, with coarse sediment particles, reflecting the strong hydrodynamic conditions and the ability of flash floods to carry materials of larger grain size to accumulate here (**Figure 5**). During the use of the dam (5000-3900a BP), the depositional environment inside the dam changed from fluvial facies to floodplain facies, and the depositional environment was relatively stable. At this time, the sediment particles were smaller, and the hydrodynamic force was weak, indicating that the completion of the Ganggongling Dam had a positive significance for regulating flash floods (**Figure 4C**). After the dam was abandoned (3900~400 a BP), the hydrodynamic force gradually weakened. To about 3200~1200 aBP, dark gray lacustrine facies deposits developed, indicating that after the dam was abandoned, the lack of manual management resulted in blockage of the drainage outlet, and the water flow in the dam was not smooth and blocked.

The documentary record shows that the construction of the dam near the ancient city of Liangzhu was several hundred years later than the ancient city, probably reflecting the fact that the ancient people of Liangzhu realized the importance of building dams by summing up their experience of the development of the Majiahong and Songze cultures in the past centuries or even two thousand years (Liu, 2008). The ancients gradually realized that ancient cities and farmlands were vulnerable to flash floods under the climate and precipitation conditions of the region.

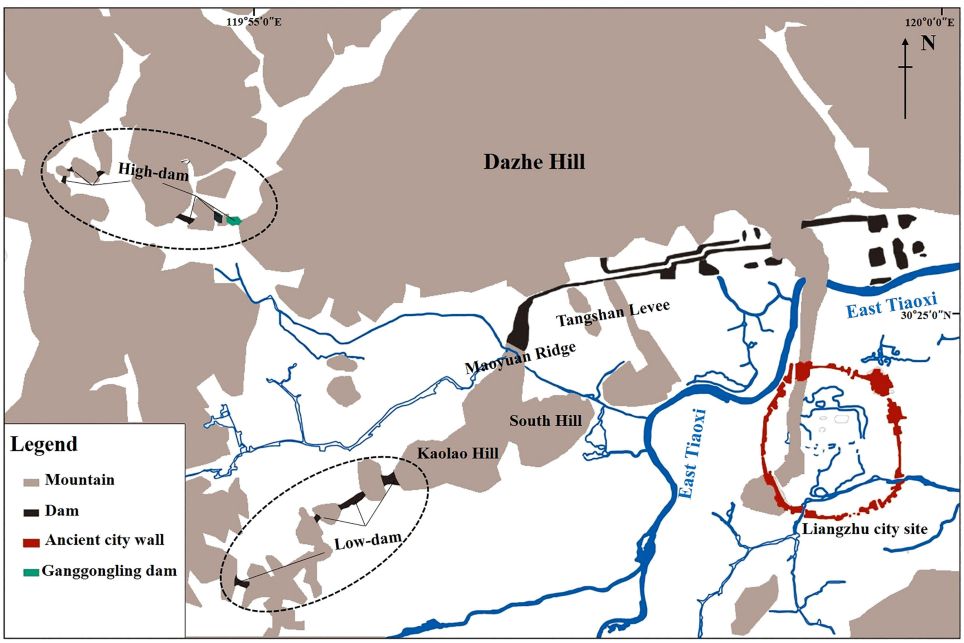

FIGURE 6 | Topographic map showing the location of Liangzhu City and the hydraulic enterprise system (Modified by Liu et al., 2014a).

Therefore, protection against surges through the construction of dams was the most basic need to protect the ancient cities and the surrounding farmland (Liu et al., 2014a).

In addition to the function of flood control and water storage, the reservoirs formed by multi-stage dams were also important transportation channels at that time (**Figure 6**). In the high-dam system, the reservoir area formed by Ganggongling, Huoling, and Zhoujiafan dams can go up the valley about 3000m when it is complete. The low-dam system can go north about 3700m when it is done and reach below Ganggongling dam, and the northeast side is connected with the Tangshan long dike, which plays a perfect role in water transportation (Liu et al., 2014; Wang and Liu, 2015). These hydraulic facilities also facilitated the development of rice agriculture, as evidenced by evidence that organic matter lenses distributed in a chalky to clayey soil matrix in rice fields at the Maoshan site may have formed under controlled flooding or irrigation (Zhuang et al., 2014).

In general, the construction of the GGL dam reflects the qualitative change in the ideology of the ancient people during the Liangzhu culture and is an essential step in the development of Neolithic society. In the process of environmental change, the ancient people no longer simply adapted to the natural environment by migrating to higher ground but actively sought to transform it (Liu et al., 2018). Thus, the emergence of ancient cities and dams resulted from the close combination of a stable environment, developed products, and social development. It also reflects the transformation of Liangzhu culture from a rice-based agricultural civilization to a high-level society with an embryonic class and social division of labor (Shi et al., 2011; Liu et al., 2017b).

Possible Driving Mechanisms Contributing to the Multi-Decadal to Centennial EASM Variations

Variations in the EASM on decades to centuries scales during the Holocene may be attributed to many factors, and solar activity is thought to be the dominant factor in EASM oscillations (Fleitmann et al., 2003; Jia et al., 2015; Zheng et al., 2015). The summer monsoon originates from low latitude ocean air mass and is greatly affected by solar radiation, so the summer monsoon responds better to solar radiation (Wehausen and Brumsack, 2002). The decades- to centuries-scale drought intervals recorded in the SC2 content and Na/K ratio of the GGL profile correlate with the time interval of solar radiation intensity (TSI) reduction inferred from cosmic ray-derived radionuclides (**Figures 7A–C**, Steinhilber et al., 2012), suggesting that solar activity conditions may control precipitation fluctuations during the Holocene in coastal eastern China. Further evidence for this proposition is provided by the significant similarity between the cyclic variation in SC2 content and the variation in solar radiation intensity recorded at $\Delta^{14}C$ (Damon and Sonett, 1991). However, the drive-response relationship within the monsoon system is difficult to explain by a single model (Ding et al., 1995; Gupta et al., 2003). Thus, we conclude that further amplification mechanisms such as the El Niño-Southern Oscillation (ENSO) in the equatorial Pacific (Marchitto et al., 2010; Lim and Fujiki, 2011; Jia et al., 2015; Park et al., 2016) may play an important role in enhancing the influence of solar radiation on EASM precipitation.

The tropical Pacific atmosphere-ocean system plays an important regulatory role between the Sun and the Earth's

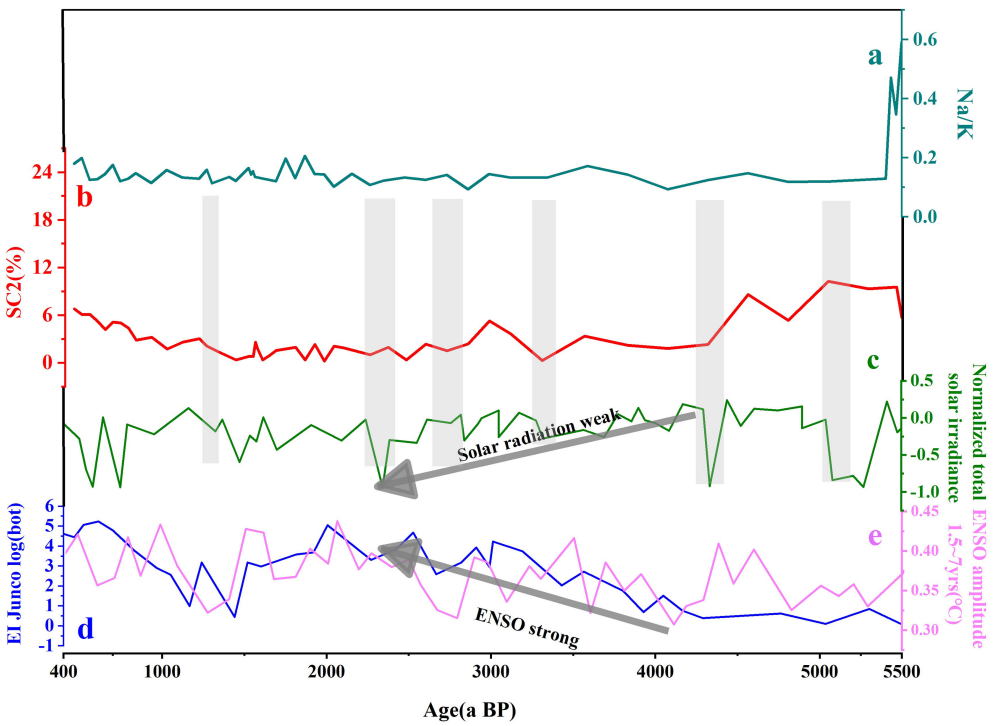

FIGURE 7 | Comparison of multi-decadal to centennial time scale climate changes recorded in GGL section **(A, B)** with potential forcing factors **(C–E)**. **(A)** Na/K ratio in the GGL section; **(B)** grain size sensitive component 2 content in the GGL section; **(C)** normalized total solar irradiance reconstructed from a cosmic ray intensity record (Steinhilber et al., 2012); **(D)** ENSO-like record from Lake El Junco indicated by the Botryococcene concentration (Conroy et al., 2008); **(E)** ENSO amplitude simulation results in the 100-year window from CCSM3 model (Liu et al., 2014b).

climate. The sea-air feedback system produces persistent El Niño-like SST anomalies when solar radiation decreases, gradually affecting the climate worldwide (Emile-Geay et al., 2007). Previous studies have shown that ENSO strongly influenced the changes in the East Asian monsoon during the Holocene, and the intensity of ENSO activity varied greatly (Conroy et al., 2008; Chen et al., 2016). At Lake El Junco in the Galápagos Islands, strong and frequent El Niño events occurred during 4000-2000 cal a B.P. and were documented by indicators such as lake grain size, staphylococcal concentration, and δ^2H (Conroy et al., 2008; Zhang et al., 2014). In addition, sea surface temperature, photosynthetic pigments, and rocky debris material in marine sediments near the Peruvian coast collectively reflect the maximum El Niño activity during the 3000-2000 cal a B.P. period (Conroy et al., 2008; Zhang et al., 2014). Our results show that the dry periods indicated by SC2 and Na/K in the GGL profiles are broadly consistent with the weakening of ENSO activity in the late Holocene (**Figures 7A, B, D, E**). In other words, this suggests that stronger ENSO can trigger significant amounts of precipitation in the Liangzhu area and also implies that ENSO activity plays a dominant role in decades to centuries of extreme climate change. In modern observations and simulations, scholars have confirmed that the increase in rainfall in the lower Yangtze River is strongly associated with enhanced ENSO activity (Tong et al., 2006; Li et al., 2011; Zeng et al., 2011). In addition, a significant increase in the frequency of ENSO-related storm events in the middle Yangtze River during the Late Holocene provides further evidence for a strong link between enhanced ENSO activity and increased precipitation in central China (Hong et al., 2006; Zhu et al., 2017). The reason may be that the improved ENSO activity (El Niño state) and the weakened solar activity lead to the negative anomaly in the Indo-Pacific warm pool SST, which induces the formation of Kelvin waves in the cold phase in the western Pacific. This causes abnormal cyclonic activity in the northwest Pacific Ocean, preventing monsoon moisture transport to the south and north of China (Jia et al., 2015; Rao et al., 2016).

CONCLUSIONS

Geochemical and grain size data from the GGL section from the Liangzhu city complex in eastern China provide a ~5500a record of paleoclimate evolution and the EASM precipitation variations. Two intervals of stronger chemical weathering indicate a humid-warm climate, occurring at 5500~3200 a BP and 1800~1200 a BP. Weak chemical weathering intensities during the 3200~1800 a BP and 1200~400 a BP suggest dry and cold climate conditions. Although some sedimentation information from the use of the dam is missing, a comparison of the sedimentation environment information inside Ganggongling Dam before its construction and after its abandonment clearly shows that the sedimentation

environment was significantly more stable after the dam was built than before. This reflects that the construction of the dam has played a positive role in regulating flash floods, not only by intercepting them to prevent them from entering the Hangjiahu Plain but also by storing water, thus alleviating the adverse effects of dry climatic conditions on human beings, and meeting the demand for water for production and living such as rice cultivation. Besides, our findings suggest that the multi-decadal to centennial EASM intensity fluctuations are primarily affected by solar irradiance. The amplification of internal forcing mechanisms, such as the El Niño-Southern Oscillation (ENSO) in the equatorial Pacific, may play an important role in enhancing the influence of solar radiation on EASM precipitation.

DATA AVAILABILITY STATEMENT

The raw data supporting the conclusions of this article will be made available by the authors, without undue reservation.

AUTHOR CONTRIBUTIONS

CZ: Conceptualization, Formal analysis, Resources, Writing original draft. LM: Formal analysis, Investigation, Editing, Funding acquisition. SS : Formal analysis, Editing. SZ: Formal analysis, Investigation, Editing. DM: Formal analysis, Investigation, Funding acquisition. All authors contributed to the article and approved the submitted version.

ACKNOWLEDGMENTS

This work was supported by the National Natural Science Foundation of China (grant number: 41771218), the National Key Research and Development Program of China (grant number:2020YFC1521605), and the National Social Science Major Foundation of China (grant number:19ZDA231). We thank the reviewers for their constructive comments that help improve an earlier version of our manuscript.

REFERENCES

Amorosi, A., Sammartino, I., and Sarti, G. (2013). Background Levels of Potentially Toxic Metals From Soils of the Pisa Coastal Plain (Tuscany, Italy) as Identified From Sedimentological Criteria. *Environ. Earth Sci.* 69 (5), 1661–1671. doi: 10.1007/s12665-012-2001-8

Banerjee, D., Murray, A S., Bøtter-Jensen, L., and Lang, A (2001). Equivalent Dose Estimation Using a Single Aliquot of Polymineral Fine Grains. *Radiation Measurements* 33, 73–94. doi: 10.1016/S1350-4487(00)00101-3

Berger, A., and Loutre, M. F. (1991). Insolation Values for the Climate of the Last 10 Million Years. *Quaternary Sci. Rev.* 10 (4), 297–317. doi: 10.1016/0277-3791(91)90033-Q

Boës, X., Rydberg, J., Martinez-Cortizas, A., Bindler, R., and Renberg, I. (2012). Evaluation of Conservative Lithogenic Elements (Ti, Zr, Al, and Rb) to Study Anthropogenic Element Enrichments in Lake Sediments. *J. Paleolimnol* 46, 75–87. doi: 10.1007/s10933-011-9515-z

Boulay, S., Colin, C., Trentesaux, A., Clain, S., Liu, Z., and Lauer-Leredde, C. (2007). Sedimentary Responses to the Pleistocene Climatic Variations Recorded in the South China Sea. *Quaternary Res.* 68 (1), 162—172. doi: 10.1016/j.yqres.2007.03.004

Boyle, J. F. (2002). Inorganic Geochemical Methods in Paleolimnology. *Tracking Environ. Change Using Lake Sediment* 2, 83–141. doi: 10.1007/0-306-47670-3_5

Chang, H., An, Z. S., Wu, F., Jin, Z. D., Liu, W. G., and Song, Y. G. (2013). An Rb/Sr Record of the Weathering Response to Environmental Changes in Westerly Winds Across the Tarim Basin in the Late Miocene to the Early Pleistocene. *Palaeogeography Palaeoclimatol. Palaeoecol.* 386 (6), 364–373. doi: 10.1016/j.palaeo.2013.06.006

Chen, S., Hoffmann, S. S., Lund, D. C., Cobb, K. M., Emile-Geay, J., and Adkins, J. F. (2016). A High-Resolution Speleothem Record of Western Equatorial Pacific Rainfall: Implications for Holocene ENSO Evolution. *Earth Planet. Sci. Lett.* 442, 61–71. doi: 10.1016/j.epsl.2016.02.050

Chen, C., Wang, J. S., Wang, Z., Peng, Y. B., Chen, X. H., Ma, X. C., et al. (2020). Variation of Chemical Index of Alteration (CIA) in the Ediacaran Doushantuo Formation and its Environmental Implications. *Precambrian Res.* 347, 105829. doi: 10.1016/j.precamres.2020.105829

Chen, Z., Zong, Y., Wang, Z., Wang, H., and Chen, J. (2008). Migration Patterns of Neolithic Settlements on the Abandoned Yellow and Yangtze River Deltas of China. *Quaternary Res.* 70 (2), 301–314. doi: 10.1016/j.yqres.2008.03.011

Che, Y. P., Xiao, H. Y., Cui, M. Y., Jiang, X. Y., and Cai, B. G. (2018). Age and Subrotational Characteristics of the Heinrich2 Event Recorded in the Stalagmite of Xianyun Cave, Minxi. *J. Sedimentol.* 36 (6), 9. doi: 10.14027/j.issn.1000-0550.2018.143

Colman, S. M., Yu, S. Y., An, Z. S., Shen, J., and Henderson, A. C. G. (2007). Late Cenozoic Climate Changes in China's Western Interior: A Review of Research on Lake Qinghai and Comparison With Other Records. *Quaternary Sci. Rev.* 26 (17-18), 2281–2300. doi: 10.1016/j.quascirev.2007.05.002

Conroy, J. L., Overpeck, J. T., Cole, J. E., Shanahan, T. M., and Steinitz-Kannan, M. (2008). Holocene Changes in Eastern Tropical Pacific Climate Inferred From a Galápagos Lake Sediment Record. *Quaternary Sci. Rev.* 27, 1166–1180. doi: 10.1016/j.quascirev.2008.02.015

Cui, M. Y., Xiao, H. Y., Sun, X. S., Hong, H., Jiang, X. Y., and Cai, B. G. (2017). Characteristics of the Heinrich 1 Abrupt Climate Event Inferred From a Speleothem Record From Xianyun Cave, Fujian Province. *Chin. Sci. Bull.* 62 (26), 11. doi: 10.1360/N972017-00091

Cullen, H. M., Demenocal, P. B., Hemming, S., Hemming, G., Brown, F. H., Guilderson, T., et al. (2000). Climate Change and the Collapse of the Akkadian Empire: Evidence From the Deep Sea. *Geology* 28 (4), 379–382. doi: 10.1130/0091-7613(2000)2<379:CCATCO>2.0.CO;2

Damon, P. E., and Sonett, C. P. (1991). "Solar and Terrestrial Components of Theatmospheric14c Variation Spectrum," in *The Sun in Time*. Eds. C. P. Sonett, M. S. Giampapa and M. S. Matthews (Tucson: University of Arizona Press), 360–388.

Davison, W. (1993). Iron and Manganese in Lakes. *Earth Sci. Rev.* 34 (2), 119–163. doi: 10.1016/0012-8252(93)90029-7

Ding, Z. L., and Yu, C. W. (1995). Dynamical Mechanisms of Monsoonal Changes in East Asia During the Quaternary Period. *Quaternary Res.* 15 (1), 63–74.

Dixit, Y., Hodell, D. A., and Petrie, C. A. (2014). Abrupt Weakening of the Summer Monsoon in Northwest India ~4100 Yr Ago. *Geology* 42 (4), 339–342. doi: 10.1130/G35236.1

Dong, J. G., Diao, W., and Kong, X. K. (2013). Variation in Uranium Isotopes of Stalagmites From Sanbao Cave, Hubei Province: Implications for Palaeoclimate. *Marine Geol. Quaternary Geol.* 33 (1), 129–136. doi: 10.3724/SP.J.1140.2013.01129

Dong, G. H., Ruo, L., Lu, M. X., Zhang, D. J., and Nathaniel, J. (2019). Evolution of Human-Environmental Interactions in China From the Late Paleolithic to the Bronze Age. *Prog. Phys. Geography: Earth Environ.* 44 (2), 233–250. doi: 10.1177/0309133319876802

Dong, J., Wang, Y., Cheng, H., Hardt, B., Edwards, R. L., Kong, X., et al. (2010). A High-Resolution Stalagmite Record of the Holocene East Asian Monsoon From Mt Shennongjia, Central China. *Holocene* 20 (2), 257–264. doi: 10.1177/0959683609350393

Du, S., Li, B., Niu, D., Zhang, D. D., Wen, X., Chen, D., et al. (2011). Age of the MGS5 Segment of the Milanggouwan Stratigraphical Section and Evolution of the Desert Environment on a Kiloyear Scale During the Last Interglacial in

China's Salawusu River Valley: Evidence From Rb and Sr Contents and Ratios. *Geochemistry* 71 (1), 87–95. doi: 10.1016/j.chemer.2010.07.002

Dykoski, C. A., Edwards, R. L., Cheng, H., Yuan, D. X., Cai, Y. J., Zhang, M. L., et al. (2005). A High-Resolution, Absolute-Dated Holocene and Deglacial Asian Monsoon Record From Dongge Cave, China. *Earth Planet. Sci. Lett.* 233 (1-2), 71–86. doi: 10.1016/j.epsl.2005.01.036

Emile-Geay, J., Cane, M., Seager, R., Kaplan, A., and Almasi, P. (2007). El Niño as a Mediator of the Solar Influence on Climate. *Paleoceanography* 22 (3), 3210. doi: 10.1029/2006PA001304

Fan, D. D., Wu, Y. J., Zhang, Y., Burr, G., Huo, M., and Li, J. (2017). South Flank of the Yangtze Delta: Past, Present, and Future. *Mar. Geol.* 392, 78–93. doi: 10.1016/j.margeo.2017.08.015

Fleitmann, D., Burns, S. J., Mudelsee, M., Neff, U., Kramers, J., Mangini, A., et al. (2003). Holocene Forcing of the Indian Monsoon Recorded in a Stalagmite From Southern Oman. *Science* 300 (5626), 1737–1739. doi: 10.1126/science.1083130

Fu, C.F., An, Z.S., Qiang, X., Bloemendal, J., Song, Y., and Chang, H (2013). Magnetostratigraphic Determination of the Age of Ancient Lake Qinghai, and Record of the East Asian Monsoon Since 4.63 Ma. *Geology* 41 (8), 875–78. doi: 10.1130/G34418.1

Fu, J. H., Li, S. X., and Niu, X. B. (2018). Paleo-Sedimentary Environmental Restoration and its Significance of Chang 7 Member of Triassic Yanchang Formation in Ordos Basin, NW China. *Petroleum Explor. Dev.* 45 (6), 998–1008. doi: 10.1016/S1876-3804(18)30104-6

Gai, C. C., Liu, Q. S., Roberts, A. P., Chou, Y. M., Zhao, X. X., Jiang, Z. X., et al. (2020). East Asian Monsoon Evolution Since the Late Miocene From the South China Sea. *Earth Planet. Sci. Lett.* 530, 115960. doi: 10.1016/j.epsl.2019.115960

Goldsmith, Y., Broecker , W.S., Xu, H., Polissar, P.J., deMenocal, P.B., Porat, N, et al. (2017). Northward Extent of East Asian Monsoon Covaries With Intensity on Orbital and Millennial Timescales. *Proc. Natl. Acad. Sci. U. S. A.* 114, 1817–21. doi: 10.1073/pnas.1616708114

González-Sampériz, P., Valero-Garcés, B. L., Moreno, A., Morellón, M., Navas, A., Machín, J., et al. (2008). Vegetation Changes and Hydrological Fluctuations in the Central Ebro Basin (Ne Spain) Since the Late Glacial Period: Saline Lake Records. *Palaeogeography Palaeoclimatol. Palaeoecol.* 259 (2), 157–181. doi: 10.1016/j.palaeo.2007.10.005

Gupta, A. K., Anderson, D. M., and Overpeck, J. T. (2003). Abrupt Changes in the Asian Southwest Monsoon During the Holocene and Their Links to the North Atlantic Ocean. *Nature* 421, 354–357. doi: 10.1038/nature01340

Hong, B., Lin, Q. H., and Hong, Y. T. (2006). Holocene Asian Monsoon, ENSO, and High Northern Latitude Climate Correlation. *Chin. Sci. Bull.* 51 (17), 8. doi: 10.1360/csb2006-51-17-1977

Huang, C., Wei, G., Li, W., and Liu, Y. (2018). A Geochemical Record of the Link Between Chemical Weathering and the East Asian Summer Monsoon During the Late Holocene Preserved in Lacustrine Sediments From Poyang Lake, Central China. *J. Asian Earth Sci.* 154, 17–25. doi: 10.1016/j.jseaes.2017.12.008

Huan, X. J., Zhang, J. P., Zhuang, Y. J., Fan, C., Wang, N. Y., Ji, X., et al. (2022). Intensification of Rice Farming and its Environmental Consequences Recorded in a Liangzhu Reservoir, China. *Quaternary Int.* 619, 39–45. doi: 10.1016/j.quaint.2022.01.012

Innes, J. B., Zong, Y., Wang, Z., and Chen, Z. (2014). Climatic and Palaeoecological Changes During the Mid-to-Late Holocene Transition in Eastern China: High-Resolution Pollen and non-Pollen Palynomorph Analysis at Pingwang, Yangtze Coastal Lowlands. *Quaternary Sci. Rev.* 99 (9), 164–175. doi: 10.1016/j.quascirev.2014.06.013

Jeong, G. Y., Cheong, C. S., and Kim, J. (2006). Rb-Sr and K-Ar Systems of Biotite in Surface Environments Regulated by Weathering Processes With Implications for Isotopic Dating and Hydrological Cycles of Sr Isotopes. *Geochimica Et Cosmochimica Acta* 70 (18), 4734–4749. doi: 10.1016/j.gca.2006.07.012

Jia, G., Bai, Y., Yang, X., Xie, L., Wei, G., Ouyang, T., et al. (2015). Biogeochemical Evidence of Holocene East Asian Summer and Winter Monsoon Variability From a Tropical Maar Lake in Southern China. *Quaternary Sci. Rev.* 111, 51–61. doi: 10.1016/j.quascirev.2015.01.002

Kalinin, P. I., Kudrevatykh, I. Y., Vagapov, I. M., Borisov, A. V., and Alekseev, A. O. (2018). Biogeochemical Processes in Steppe Landscapes of the Ergeni Upland in the Holocene. *Eurasian Soil Sci.* 51 (5), 495–505. doi: 10.1134/S1064229318050058

Kennett, D. J., Breitenbach, S., Aquino, V. V., Asmerom, Y., Awe, J., Baldini, J., et al. (2012). Development and Disintegration of Maya Political Systems in Response to Climate Change. *Science* 338 (6108), 788–791. doi: 10.1126/science.1226299

Kidder, T. R., Adelsberger, K. A., Arco, L. J., and Schilling, T. M. (2008). Basin-Scale Reconstruction of the Geological Context of Human Settlement: An Example From the Lower Mississippi Valley, USA. *Quaternary Sci. Rev.* 27 (11-12), 1255–1270. doi: 10.1016/j.quascirev.2008.02.012

Kirwan, M. L., and Megonigal, J. P. (2013). Tidal Wetland Stability in the Face of Human Impacts and Sea-Level Rise. *Nature* 504 (7478), 53–60. doi: 10.1038/nature12856

Kronberg, B. I., Nesbitt, H. W., and Lam, W. W. (1986). Upper Pleistocene Amazon Deep-Sea Fan Muds Reflect Intense Chemical Weathering of Their Mountainous Source Lands. *Chem. Geol.* 54 (3-4), 283–294. doi: 10.1016/0009-2541(86)90143-9

Kutzbach, J. E. (1981). Monsoon Climate of the Early Holocene: Climate Experiment With the Earth's Orbital Parameters for 9000 Years Ago. *Science* 214 (4516), 59–61. doi: 10.1126/science.214.4516.59

Kylander, M. E., Ampel, L., Wohlfarth, B., and Veres, D. (2011). High-Resolution X-Ray Fluorescence Core Scanning Analysis of Les Echets (France) Sedimentary Sequence: New Insights From Chemical Proxies. *J. Quaternary Sci.* 26 (1), 109–117. doi: 10.1002/jqs.1438

Lai, Z., and Brückner, H. (2008). Effects of Feldspar Contamination on Equivalent Dose and the Shape of Growth Curve for OSL of Silt-Sized Quartz Extracted From Chinese Loess. *Geochronometria* 30, 49–53. doi: 10.2478/v10003-008-0010-0

Lim, J., and Fujiki, T. (2011). Vegetation and Climate Variability in East Asia Driven by Low Latitude Oceanic Forcing During the Middle to Late Holocene. *Quaternary Sci. Rev.* 30 (19-20), 2487–2497. doi: 10.1016/j.quascirev.2011.05.013

Ling, G. J., Ma, C. M., Yang, Q., Hu, Z. J., Zheng, H. B., Liu, B., et al. (2021). Landscape Evolution in the Liangzhu Area Since the Early Holocene: A Comprehensive Sedimentological Approach. *Palaeogeography Palaeoclimatol. Palaeoecol.* 562, 110141. doi: 10.1016/j.palaeo.2020.110141

Liu, B. (2008). Report of Archaeological Excavation on Liangzhu City-Site in Hangzhou City for the Period 2006~2007. *Archaeology* 7, 586—579.

Liu, T., Liu, Y., Sun, Q., Zong, Y., Finlayson, B., and Chen, Z. (2017b). Early Holocene Groundwater Table Fluctuations in Relation to Rice Domestication in the Middle Yangtze River Basin, China. *Quaternary Sci. Rev.* 155, 79–85. doi: 10.1016/j.quascirev.2016.11.015

Liu, Z. Y., Lu, Z. Y., Wen, X. Y., Otto-Bliesner, B. L., Timmermann, A., and Cobb, K. M. (2014b). Evolution and Forcing Mechanisms of El Nino Over the Past 21,000 Years. *Nature* 515, 550–553. doi: 10.1038/nature13963

Liu, B., Wang, N., Chen, M., Wu, X., Mo, D., Liu, J., et al. (2017a). Earliest Hydraulic Enterprise in China 5,100 Years Ago. *Proc. Natl. Acad. Sci.* 114 (52), 13637–13642. doi: 10.1073/pnas.1710516114

Liu, B., Wang, N. Y., Zheng, Y. F., Chen, X. G., Zhou, W. L., Yan, K. K., et al. (2014a). Findings of Archaeological Survey of Prehistoric City at Liangzhu During 2006-2013. *Southeast Culture* 2, 31–38.doi: 10.3969/j.issn.1001-179X.2017.06.010

Liu, S., Shi, X., Liu, Y., Wu, Y., Yang, G., and Wang, X (2013). Holocene Paleoclimatic Reconstruction Based on Mud Deposits on the Inner Shelf of the East China Sea. *J. Asian Earth Sci.* 69 113–20. doi: 10.1016/j.jseaes.2013.01.003

Liu, Y., Sun, Q., Fan, D., Dai, B., Ma, F., Xu, L, et al. (2018). Early to Middle Holocene Sea Level Fluctuation, Coastal Progradation and the Neolithic Occupation in the Yaojiang Valley of Southern Hangzhou Bay, Eastern China. *Quat. Sci. Rev.* 189, 91–104. doi: 10.1016/j.quascirev.2018.04.010

Li, X., Yang, H., Yao, Y., Chen, Y., and Liu, W. (2016). Precipitation Changes Recorded in the Sedimentary Total Organic Carbon Isotopes From Lake Poyang in the Middle and Lower Yangtze River, Southern China Over the Last 1600 Years. *Quaternary Int.* 425 (2), 292–300. doi: 10.1016/j.quaint.2016.07.020

Li, W., Zhai, P., and Cai, J. (2011). Research on the Relationship of ENSO and the Frequency of Extreme Precipitation Events in China. *Adv. Climate Change Res.* 2 (2), 101–107. doi: 10.3724/SP.J.1248.2011.00101

Li, P., Zhang, C. X., Wu, H. B., and Gao, Z. W. (2022). Geochemical Characteristics of Holocene Loess-Paleosol Sequences in Central Chinese

Loess Plateau and Their Implications for East Asian Monsoon Evolution. *Quaternary Int.* 616, 99–108. doi: 10.1016/j.quaint.2021.10.017

Long, T., Qin, J., Atahan, P., Mooney, S., and Taylor, D. (2014). Rising Waters: New Geoarchaeological Evidence of Inundation and Early Agriculture From Former Settlement Sites on the Southern Yangtze Delta, China. *Holocene* 24 (5), 546–558. doi: 10.1177/0959683614522309

Lu, P. Y. (2008). *Study on the Sedimentary Structure and Spatial Spreading Pattern of the Quaternary in Hangzhou* (Hangzhou: Zhejiang University).

Macklin, M. G., Toonen, W. H., Woodward, J. C., Williams, M. A., Flaux, C., Marriner, N., et al. (2015). A New Model of River Dynamics, Hydroclimatic Change and Human Settlement in the Nile Valley Derived From Meta-Analysis of the Holocene Fluvial Archive. *Quaternary Sci. Rev.* 130, 109–123. doi: 10.1016/j.quascirev.2015.09.024

Marchitto, T. M., Muscheler, R., Ortiz, J. D., Carriquiry, J. D., and van Geen, A. (2010). Dynamical Response of the Tropical Pacific Ocean to Solar Forcing During the Early Holocene. *Science* 330 (6009), 1378–1381. doi: 10.1126/science.1194887

Moreno, A., Giralt, S., Valero-Garcés, B., Sáez, A., Bao, R., Prego, R., et al. (2007). A 14 Kyr Record of the Tropical Andes: The Lago Chungará Sequence (18°s, Northern Chilean Altiplano). *Quaternary Int.* 161 (1), 4–21. doi: 10.1016/j.quaint.2006.10.020

Mu, Y., Qin, X, Zhang, , and Xu, L. (2016). Holocene Climate Change Evidence From High Resolution Loess/paleosol Records and the Linkage to Fire-Climate Change-Human Activities in the Horqin Dunefield in Northern China. *J. Asian Earth Sci.* 121, 1–8. doi: 10.1016/j.jseaes.2016.01.017

Munoz, S. E., Gruley, K. E., and Massie, A. (2015). Cahokia's Emergence and Decline Coincided With Shifts of Flood Frequency on the Mississippi River. *Proc. Natl. Acad. Sci. U.S.A* 112, 6319–6324. doi: 10.1073/pnas.1501904112

Nicholls, R. J., and Cazenave, R. (2010). Sea-Level Rise and its Impact on Coastal Zones. *Science* 328 (5985), 1517–1520. doi: 10.1126/science.118578

Nienhuis, J. H., Ashton, A. D., Edmonds, D. A., Hoitink, A., and Törnqvist, T. E. (2020). Global-Scale Human Impact on Delta Morphology has Led to Net Land Area Gain. *Nature* 577 (7791), 514–518. doi: 10.1038/s41586-019-1905-9

Núñez, L., Grosjean, M., and Cartajena, I. (2002). Human Occupations and Climate Change in the Punade Atacama, Chile. *Science* 298, 821–824. doi: 10.1126/science.1076449

Oldfield, F., Bloemendal, J., and Thompson, R. (1979). Magnetic Measurements Used to Access Sediment Influx at Llyn Goddionduon. *Nature* 280, 50–53. doi: 10.1038/280050a0

Park, J., Shin, Y. H., and Byrne, R. (2016). Late-Holocene Vegetation and Climate Change in Jeju Island, Korea and its Implications for ENSO Influences. *Quaternary Sci. Rev.* 153, 40–50. doi: 10.1016/j.quascirev.2016.10.011

Perri, F. (2020). Chemical Weathering of Crystalline Rocks in Contrasting Climatic Conditions Using Geochemical Proxies: An Overview. *Palaeogeography Palaeoclimatol. Palaeoecol.* 556, 109873. doi: 10.1016/j.palaeo.2020.109873

Rao, Z., Li, Y., Zhang, J., Jia, G., and Chen, F. (2016). Investigating the Long-Term Palaeoclimatic Controls on the δd and δ18o of Precipitation During the Holocene in the Indian and East Asian Monsoonal Regions. *Earth Sci. Rev.* 159, 292–305. doi: 10.1016/j.earscirev.2016.06.007

Rolett, B. V., Zheng, Z., and Yue, Y. F. (2011). Holocene Sea-Level Change and the Emergence of Neolithic Seafaring in the Fuzhou Basin (Fujian, China). *Quaternary Sci. Rev.* 30 (7-8), 788–797. doi: 10.1016/j.quascirev.2011.01.015

Rosenbaum, J. G., and Reynolds, R. L. (2004). Basis for Paleoenvironmental Interpretation of Magnetic Properties of Sediment From Upper Klamath Lake (Oregon): Effects of Weathering and Mineralogical Sorting. *J. Paleolimnol.* 31, 253–265. doi: 10.1023/B:JOPL.0000019228.46421.f4

Ryabogina, N. E., Afonin, A. S., Ivanov, S. N., Li, H. C., and Nikolaenko, S. A. (2019). Holocene Paleoenvironmental Changes Reflected in Peat and Lake Sediment Records of Western Siberia: Geochemical and Plant Macrofossil Proxies. *Quaternary Int.* 528, 73–87. doi: 10.1016/j.quaint.2019.04.006

Shi, C. X., Mo, D. W., Li, C. H., Liu, B., Mao, L. J, and Li, M. (2011). The Relationship Between Environmental Evolution and Human Activities of the Liangzhu Site Group Zhejiang Province, China. . *Earth Sci. Front.* 18 (13), 347–56.

Stankevica, K., Klavins, M., Vincevica-Gaile, Z., Kalnina, L., and Kaup, E. (2020). Accumulation of Metals and Changes in Composition of Freshwater Lake Organic Sediments During the Holocene. *Chem. Geol.* 539, 119502. doi: 10.1016/j.chemgeo.2020.119502

Stanley, D. J., and Chen, Z. (1996). Neolithic Settlement Distributions as a Function of Sea Level Controlled to Pography in the Yangtze Delta, China. *Geology* 24 (24), 1083–1086. doi: 10.1130/0091-7613(1996)024<1083:NSDAAF>2.3.CO;2

Steinhilber, F., Abreu, J. A., Beer, J., Brunner, I., Christl, M., Fischer, H., et al. (2012). 9,400 Years of Cosmic Radiation and Solar Activity From Ice Cores and Tree Rings. *Proc. Natl. Acad. Sci.* 109 (16), 5967–5971. doi: 10.1073/pnas.1118965109

Sun, Q., Liu, Y., Wünnemann, B., Peng, Y., and Chen, Z. (2019). Climate as a Factor for Neolithic Cultural Collapses Approximately 4000 Years BP in China. *Earth Sci. Rev.* 197, 102915. doi: 10.1016/j.earscirev.2019.102915

Timmermann, A., and Friedrich, T. (2016). Late Pleistocene Climate Drivers of Early Human Migration. *Nature* 538 (7623), 92–95. doi: 10.1038/nature19365

Tong, J., Zhang, Q., Zhu, D. M., and Wu, Y. J. (2006). Yangtze Floods and Droughts (China) and Teleconnections With ENSO Activities, (1470-2003). *Quaternary Int.* 144 (1), 29–37. doi: 10.1016/j.quaint.2005.05.010

Turney, C., and Brown, H. (2007). Catastrophic Early Holocene Sea-Level Rise, Human Migration, and the Neolithic Transition in Europe. *Quaternary Sci. Rev.* 26 (17-18), 2036–2041. doi: 10.1016/j.quascirev.2007.07.003

Wang, P., Du, Y. S., Yu, W. C., Algeo, T. J., Zhou, Q., Xu, Y., et al. (2020). The Chemical Index of Alteration (CIA) as a Proxy for Climate Change During Glacial-Interglacial Transitions in Earth History. *Earth Sci. Rev.* 201, 103032. doi: 10.1016/j.earscirev.2019.103032

Wang, N. Y., and Liu, B. (2015). Archaeological Investigation of the Peripheral Hydraulic System of the Ancient City of Liangzhu in Hangzhou. *Archaeology* 1), 3–13.

Wang, Z., Ryves, D. B., Lei, S., Nian, X., Lv, Y., Tang, L., et al. (2018). Middle Holocene Marine Flooding and Human Response in the South Yangtze Coastal Plain, East China. *Quaternary Sci. Rev.* 187, 80–93. doi: 10.1016/j.quascirev.2018.03.001

Wang, K. F., and Zhang, Y. L. (1981). Inferring the Climatic Changes in the Shanghai-Hangzhou Region for More Than 10,000 Years Based on Sporopollen Analysis. *Historical Geography* 1, 6.

Wehausen, R., and Brumsack, H. J. (2002). Astronomical Forcing of the East Asian Monsoon Mirrored by the Composition of Pliocene South China Sea Sediments. *Earth Planet. Sci. Lett.* 201 (3-4), 621–636. doi: 10.1016/S0012-821X(02)00746-X

Wu, X. D., Shen, J., and Wang, Y. (2011). Paleoenvironmental Evolution Since the Holocene as Reflected by Lacustrine Marl Lake Sediments. *Marine Geol. Quaternary Geol.* 31 (4), 8.

Xu, G. L. (2012). *Changes in the Structure and Connectivity of the Taihu Plain and Their Effects on Hydrological Processes* (Nanjing: Nanjing University).

Yang, S. Y., Tang, M., Yim, W. W. S., Zong, Y. Q., Huang, G. Q., Switzer, A. D., et al. (2011). Burial of Organic Carbon in Holocene Sediments of the Zhujiang (Pearl River) and Changjiang (Yangtze River) Estuaries. *Marine Chem.* 123 (1-4), 1–10. doi: 10.1016/j.marchem.2010.07.001

Yang, T., Zhang, J., and Shi, W. (2002). The Characteristics of Tidal Current Distribution in Zhapu Section of the Hangzhou Bay. *Donghai Mar. Sci.* 20 (4), 1–7. . doi: 10.3969/j.issn.1001-909X.2002.04.001

Yan, Z. M., Lu, X. X., and Zheng, G. A. (1959). Problems of Comprehensive Utilization of Soil and Water Resources in the Hangjia Lake Area. *Acta Geographica Sin.* 04), 299–312.

Yao, Y., Yang, H., Liu, W., Li, X., and Chen, Y. (2015). Hydrological Changes of the Past 1400 Years Recorded in δd of Sedimentary N-Alkanes From Poyang Lake, Southeastern China. *Holocene* 25, 1068–1075. doi: 10.1177/0959683615576231

Yi, S., Saito, Y., Oshima, H., Zhou, Y., and Wei, H. (2003). Holocene Environmental History Inferred From Pollen Assemblages in the Huanghe (Yellow River) Delta, China: Climatic Change and Human Impact. *Quaternary Sci. Rev.* 22, 609–628. doi: 10.1016/S0277-3791(02)00086-0

Yi, S., Saito, Y., and Yang, D. Y. (2006). Palynological Evidence for Holocene Environmental Change in the Changjiang (Yangtze River) Delta, China. *Palaeogeography Palaeoclimatol. Palaeoecol.* 241, 103–117. doi: 10.1016/j.palaeo.2006.06.016

Yi, S., Saito, Y., Zhao, Q. H., and Wang, P. X. (2003). Vegetation and Climate Changes in the Changjiang (Yangtze River) Delta, China, During the Past

13,000 Years Inferred From Pollen Records. *Quaternary Sci. Rev.* 22, 1501–1519. doi: 10.1016/S0277-3791(03)00080-5

Zeng, X., Li, B., Feng, F., Liu, X., and Zhou, T. (2011). East China Summer Rainfall During ENSO Decaying Years Simulated by a Regional Climate Model. *Atmos. Oceanic Sci. Lett.* 2011 (4), 91–97. . doi: 10.1080/16742834.2011.11446908

Zhang, Y. L. (2005). Study on the Late Quaternary Spore Powder and Paleoenvironment in Dianshan Lake Area. *J. Tongji University: Natural Sci. Edition* 33 (2), 6. doi: 10.3321/j.issn:0253-374X.2005.02.024

Zhang, Z. H., Leduc, G., and Sachs, J. P. (2014). El Niño's Evolution During the Holocene Revealed by a Biomarker Rain Gauge in the Galápagos Islands. *Earth Planet. Sci. Lett.* 404, 420–434. doi: 10.1016/j.epsl.2014.07.013

Zheng, Y. H., Li, Q. Y., Wang, Z. Z., Naafs, B. D. A., Yu, X. F., and Pancost, R. D. (2015). Peatland GDGT Records of Holocene Climatic and Biogeochemical Responses to the Asian Monsoon. *Organic Geochemistry* 87, 86–95. doi: 10.1016/j.orggeochem.2015.07.012

Zhuang, Y., Ding, P., and French, C. (2014). Water Management and Agricultural Intensification of Rice Farming at the Late-Neolithic Site of Maoshan, Lower Yangtze River, China. *Holocene* 24, 531–545. doi: 10.1177/0959683614522310

Zhu, Z., Feinberg, J. M., Xie, S., Bourne, M. D., Huang, C., and Hu, C. (2017). Holocene ENSO-Related Cyclic Storms Recorded by Magnetic Minerals in Speleothems of Central China. *Proc. Natl. Acad. Sci.* 114 (5), 852–857. doi: 10.1073/pnas.1610930114

Zong, Y., Chen, Z., Innes, J. B., Chen, C., Wang, Z., and Wang, H. (2007). Fire and Flood Management of Coastal Swamp Enabled First Rice Paddy Cultivation in East China. *Nature* 449 (7161), 459–462. doi: 10.1038/nature06135

Zong, Y., Wang, Z., Innes, J., and Chen, Z. (2012). Holocene Environmental Change and Neolithic Rice Agriculture in the Lower Yangtze Region of China: A Review. *Holocene* 22 (6), 623–635. doi: 10.1177/0959683611409775

Conflict of Interest: The authors declare that the research was conducted in the absence of any commercial or financial relationships that could be construed as a potential conflict of interest.

Publisher's Note: All claims expressed in this article are solely those of the authors and do not necessarily represent those of their affiliated organizations, or those of the publisher, the editors and the reviewers. Any product that may be evaluated in this article, or claim that may be made by its manufacturer, is not guaranteed or endorsed by the publisher.